

Tunable Bragg filter based on polymer/silica hybrid waveguide platform

Xinyuan Zhang(张鑫源), Daming Zhang(张大明), Xinjian Zhang(张鑫健), Guoyan Zeng(曾国宴), and Yuexin Yin(尹悦鑫)

Citation: Chin. Phys. B, 2026, 35 (**7**): 078401. DOI: 10.1088/1674-1056/ae0b3b
http://cpb.iphy.ac.cn; http://iopscience.iop.org/cpb

What follows is a list of articles you may be interested in

Unveiling the in-plane anisotropic dielectric waveguide modes in α-MoO_3 flakes

Ying Liao(廖莹) and Jianing Chen(陈佳宁)
Chin. Phys. B, 2024, 33 (**7**): 078401. DOI: 10.1088/1674-1056/ad3dd7

Tunable superconducting resonators via on-chip control of local magnetic field

Chen-Guang Wang(王晨光), Wen-Cheng Yue(岳文诚), Xuecou Tu(涂学凑), Tianyuan Chi(迟天圆), Tingting Guo(郭婷婷), Yang-Yang Lyu(吕阳阳), Sining Dong(董思宁), Chunhai Cao(曹春海), Labao Zhang(张蜡宝), Xiaoqing Jia(贾小氢), Guozhu Sun(孙国柱), Lin Kang(康琳), Jian Chen(陈健), Yong-Lei Wang(王永磊), Huabing Wang(王华兵), and Peiheng Wu(吴培亨)
Chin. Phys. B, 2024, 33 (**5**): 058402. DOI: 10.1088/1674-1056/ad2f21

A low-cost invasive microwave ablation antenna with a directional heating pattern

Zhang Wen(文章), Xian-Qi Lin(林先其), Chen-Nan Li(李晨楠), and Yu-Lu Fan(樊钰璐)
Chin. Phys. B, 2022, 31 (**3**): 038401. DOI: 10.1088/1674-1056/ac1e1b

Integrated superconducting circuit for qubit and resonator protection

Xiao-Pei Yang(杨晓沛), Zhi-Kun Han(韩志坤), Shu-Qing Song(宋树清), Wen Zheng(郑文), Dong Lan(兰栋), Xin-Sheng Tan(谭新生), and Yang Yu(于扬)
Chin. Phys. B, 2021, 30 (**7**): 078403. DOI: 10.1088/1674-1056/ac003d

Compact NbN resonators with high kinetic inductance

Xing-Yu Wei(魏兴雨), Jia-Zheng Pan(潘佳政), Ya-Peng Lu(卢亚鹏), Jun-Liang Jiang(江俊良), Zi-Shuo Li(李子硕), Sheng Lu(卢盛), Xue-Cou Tu(涂学凑), Qing-Yuan Zhao(赵清源), Xiao-Qing Jia(贾小氢), Lin Kang(康琳), Jian Chen(陈健), Chun-Hai Cao(曹春海), Hua-Bing Wang(王华兵), Wei-Wei Xu(许伟伟), Guo-Zhu Sun(孙国柱), and Pei-Heng Wu(吴培亨)
Chin. Phys. B, 2020, 29 (**12**): 128401. DOI: 10.1088/1674-1056/abc2b8

Tunable Bragg filter based on polymer/silica hybrid waveguide platform

Xinyuan Zhang(张鑫源)[1], Daming Zhang(张大明)[1], Xinjian Zhang(张鑫健)[1], Guoyan Zeng(曾国宴)[1], and Yuexin Yin(尹悦鑫)[1,2,†]

[1] *State Key Laboratory of Integrated Optoelectronics, College of Electronic Science and Engineering, Jilin University, Changchun* 130012, *China*
[2] *Institute for Materials Chemistry and Engineering, Kyushu University,* 6-1 *Kasuga-koen Kasuga, Fukuoka* 816-8580, *Japan*

(Received 4 August 2025; revised manuscript received 18 September 2025; accepted manuscript online 25 September 2025)

Owing to its compact footprint and superior filter properties, the Bragg grating filter is attractive for applications in optical communications. In this research, we conducted a detailed analysis of the influence of Bragg grating parameters on its functionality and experimentally validated our findings on a simple and low-cost polymer/silica hybrid waveguide platform. The best extinction ratio of 26.3 dB is obtained when the period is 6.63 μm and the number of periods is 200. The full width at half maximum of the grating is 0.35 nm at 1544.74 nm. Tuning efficiency reaches 29.6 pm/mW owing to the high thermo-optical efficiency of the polymer. Finally, we measure the rise and fall times of the grating to be 280 μs. The proposed grating shows great potential in flexible and reconfigurable optical networks.

Keywords: waveguide, polymer, filter, integrated optics

PACS: 84.40.Az, 84.30.Vn, 42.82.–m, 42.82.Ds

DOI: 10.1088/1674-1056/ae0b3b **CSTR:** 32038.14.CPB.ae0b3b

1. Introduction

Tunable optical filters, as the backbones of optical communication networks, are highly demanded for wide applications such as reconfigurable wavelength (de)multiplexing, tunable lasers as well as spectroscopic sensing.[1–3] Compared with asymmetric Mach–Zehnder interferometers[4] and micro-ring resonator filters,[5] waveguide Bragg grating (WBG), using periodic waveguide structure, reflects light at specific wavelengths with the advantages of free spectral range (FSR)-free, compact footprint and deep extinction properties.[6,7] Till now, WBG filters have been demonstrated on many kinds of material platforms such as silicon on insulator (SOI),[8] silica on silicon,[9] and polymer.[10] On the SOI platform, researchers have successfully developed and verified a grating filter based on cladding modulation. This device consists of 20 spectral notches with non-uniform spacing, where each notch has a 3 dB bandwidth ($\Delta\lambda_{3\ \mathrm{dB}}$) as narrow as 210 pm.[11] Similarly, subwavelength multimode waveguide Bragg grating technology assisted by adiabatic directional couplers successfully constructs a narrowband silicon-based photonic filter, ultimately achieving excellent performance: $\Delta\lambda_{3\ \mathrm{dB}}$ of 0.51 nm and an extremely high side-mode suppression ratio (SMSR) of 16.6 dB. Meanwhile, this device exhibits an infinite FSR in the C-band.[12] Regarding the polymer platform, researchers have realized narrower bandwidths and higher SMSR by adopting a two-stage cascaded Bragg grating structure. Experimental verification shows that the device maintains a 20 dB bandwidth of 1.0 nm and an SMSR of 35 dB over the entire wavelength tuning range.[13] The high refractive index of silicon makes its devices compact and suitable for large-scale integration, but low fabrication tolerance and coupling efficiency limit its applications.[14] Especially for Bragg gratings on the SOI platform, the period is usually hundreds of nanometers. Electron beam lithography or deep ultraviolet (UV) lithography technologies are necessary for fabrication, which will seriously increase the cost. Silica-based and polymer-based planar lightwave circuit (PLC) technologies have similar refractive indices and micrometer-scale waveguide geometries. Waveguide devices of this size can be easily achieved through traditional UV lithography, which will dramatically lower the cost. Compared with silica, a high thermo-optic coefficient (TOC) polymer-based PLC platform offers a low-cost, easy-fabrication, and power-efficient platform for tunable optical devices.[15] Moreover, polymer is attractive in various sensing applications.[16] However, due to the small period size, polymer-based Bragg grating devices are difficult to fabricate. In this paper, in order to satisfy the fabrication resolution, we design and fabricate a high-order Bragg grating filter, so that the period is up to several micrometers. We conducted a detailed analysis of the influence of Bragg grating parameters on its functionality and experimentally validated our findings on a simple and low-cost polymer/silica hybrid waveguide platform. The device is fabricated through traditional low-cost UV lithography technology. The results for period numbers $N_\mathrm{p} = 100$ and $N_\mathrm{p} = 200$ are compared with a period length (Λ) of 6.63 μm. The devices exhibit extinction ratios

†Corresponding author. E-mail: yxyin@jlu.edu.cn

© 2026 Chinese Physical Society and IOP Publishing Ltd. All rights, including for text and data mining, AI training, and similar technologies, are reserved.

(*ER*) and 3-dB bandwidths ($\Delta\lambda_{3\ \mathrm{dB}}$) of 8.67 dB/1.3 nm and 26.3 dB/0.35 nm at the transmission peaks (λ) of 1544.22 nm and 1544.74 nm, respectively. The tuning efficiencies are 27.4 pm/mW and 29.6 pm/mW. Finally, we measure the dynamic response of the Bragg grating. The rise and fall times are 280 μs. The compact and high-efficiency Bragg grating shows potential applications in optical communication and sensing systems. In optical communication systems, it can be used as a tunable filter to dynamically adjust the central wavelength and also be employed in wavelength division multiplexing systems to achieve dynamic wavelength selection. In sensing systems, gratings can utilize their characteristic of wavelength varying with the external environment to realize high-sensitivity sensing.

2. Design and simulation of WBG filter

The schematic of the proposed WBG is illustrated in Fig. 1. There are several key parameters for the WBG, including the width of units (W_1), the period length (Λ), the length of the grating (L_1), the length of the waveguide section of a single grating (W_2), the duty cycle of the grating (D), and the thickness of the waveguide (H). The cross-section of the polymer/silica hybrid waveguide is illustrated in Fig. 1(b). The materials for lower cladding, core layer, and upper cladding are silica, SU-8, and polymethyl methacrylate (PMMA), whose refractive indices at 1550 nm are 1.445, 1.58, and 1.476, respectively. We coat an aluminum layer above PMMA as electrodes to tune the central wavelength of the filter. The geometry of the single-mode waveguide is 3×3 μm^2.[2,17,18] The lower refractive index difference requires a wider waveguide to confine light within the WBG region. Therefore, we introduce tapers between single-mode waveguides and WBG regions to reduce the loss caused by mode mismatch. As shown in Fig. 1(c), the taper is expanded to 8 μm (W_1) with a length (L_2) of 150 μm linearly. To increase coupling efficiency, we introduce a 200-μm-length (L_3) taper with a width of 16 μm (W_3) at the edges of the chip.

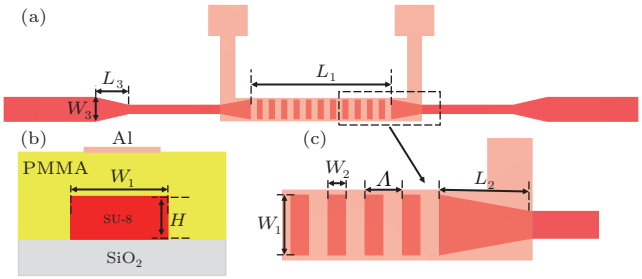


Fig. 1. (a) Schematic of the WBG. (b) Cross-section of the single-mode waveguide. (c) Enlarged schematic of the taper structures.

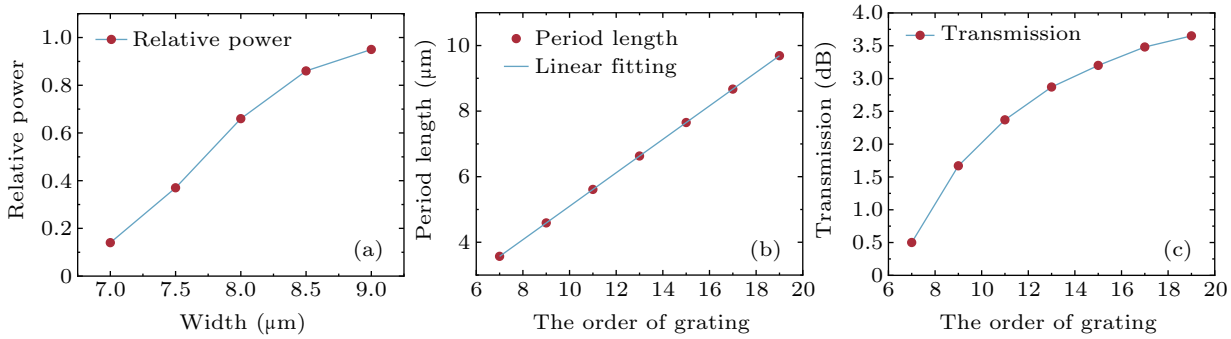


Fig. 2. (a) The fitting curve of reflectivity varying with W when $N_\mathrm{p} = 100$. (b) The fitting line between N_p and λ when $W = 8$ μm and $\lambda = 1550$ nm. (c) The fitting curve of transmission loss varying with m at 1535 nm when $N_\mathrm{p} = 100$.

Key parameters of a Bragg grating are the central wavelength (λ), $\Delta\lambda_{3\ \mathrm{dB}}$, and *ER*. Among them, the central wavelength is related to the order of the grating (m), the grating period length (Λ), and the effective refractive index (n_eff) of the grating. There is an equation[19]

$$m\lambda = 2n_\mathrm{eff}\Lambda. \tag{1}$$

The effective refractive index is related to the core-layer material used, the grating width, and the grating etching depth. To simplify the process and address the issue of waveguide rounded corners caused by wet etching, we adopt a fully etched grating structure. Figure 2(a) shows the relationship between the unit width (W_1) and the reflectivity when the number of periods (N_p) is 100. To ensure higher reflectivity while maintaining a compact footprint, we choose a waveguide with a unit width (W_1) of 8 μm. When the duty cycle (D) of the WBG is determined to be 0.5, the relationship between m and Λ at the central wavelength of 1550 nm is shown in Fig. 2(b). In Fig. 2(c), we simulate the relationship between m and the grating transmission loss at a non-central wavelength (taking 1535 nm as an example) when the number of periods is $N_\mathrm{p} = 100$. It is found that as m increases, the transmission loss of the grating increases. The reason is that as m increases, the grating length increases, leading to additional scattering loss.[20] Meanwhile, a smaller value of m ensures a shorter grating length, thereby enhancing device integration. However, due to fabrication limitations, a short grating length makes the process difficult. Taking the trade-off between inte-

gration and fabrication into account, we adopt the design parameters of the Bragg grating with $m = 13$ and $\Lambda = 6.63$ μm. The key parameters used are summarized in Table 1.

Table 1. The key parameters of grating.

Period (Λ)	Unit width (W_1)	Number of periods (N_p)	Order of grating (m)	Duty cycle (D)
6.63 μm	8 μm	100/200	13	0.5

Higher reflectivity corresponds to a larger *ER*. The reflectivity (R) of the Bragg grating is determined by[19]

$$R = \frac{|\kappa^2| \sinh^2(sL)}{s^2 \cosh^2(sL) + (\Delta\beta/2)^2 \sinh^2(sL)}. \tag{2}$$

Here, the parameter s represents the coupling mismatch parameter, and its expression can be written as

$$s = \sqrt{\kappa^2 - \left(\frac{\Delta\beta}{2}\right)^2}. \tag{3}$$

Here, κ represents the grating coupling coefficient. For κ, there is also a formula[16]

$$\kappa = \frac{2(n_{\text{eff1}} - n_{\text{eff2}})}{\lambda}. \tag{4}$$

Here, n_{eff1} and n_{eff2} are the effective refractive indices of the grating layer and the etched layer, respectively. $\Delta\beta$ is the phase mismatch parameter, which can be calculated as

$$\Delta\beta = 2\pi n_{\text{eff}} \left(\frac{1}{\lambda_1} - \frac{1}{\lambda}\right), \tag{5}$$

where λ_1 represents the actual incident wavelength. When λ_1 satisfies the Bragg condition, $\Delta\beta = 0$. When the grating length L is infinitely long, R decreases as $\Delta\beta$ increases. When the phase matching condition $\Delta\beta = 0$ is satisfied, the reflectance tends to 1. Therefore, the maximum reflectance ($R_{\max}$) is given by[19]

$$R_{\max} = \tanh^2(|\kappa|L). \tag{6}$$

Since κ has been determined, $R_{\max}$ varies with L. As for the key parameter $\Delta\lambda_{3\text{ dB}}$ of the Bragg grating, it is expressed by[19]

$$\Delta\lambda_{3\text{ dB}} = \frac{2\lambda}{n_{\text{eff}}} \sqrt{\left(\frac{\kappa L}{\pi}\right)^2 - \left(\frac{\delta L}{\pi}\right)^2}. \tag{7}$$

Here, δ represents the detuning parameter, reflecting the deviation between λ and λ_1. It can be expressed as

$$\delta = \frac{2\pi n_{\text{eff}}}{\lambda} - \frac{\pi}{\Lambda}. \tag{8}$$

For *ER*, the following expression is used:[19]

$$ER = 10 \log_{10}\left(\frac{R_1}{R_2}\right). \tag{9}$$

Here, R_1 and R_2 represent the peak reflectance and valley reflectance in the reflection spectrum, respectively.

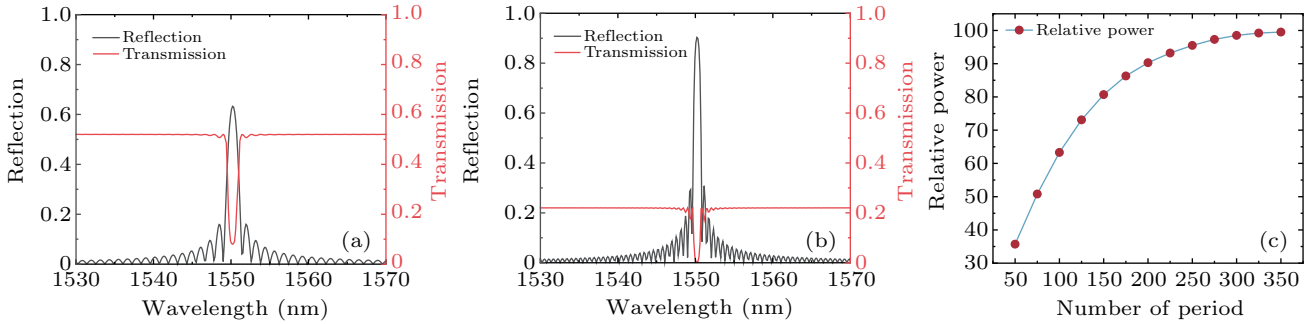


Fig. 3. Transmission and reflection spectra of (a) $N_p = 100$ and (b) $N_p = 200$ at $\Lambda = 6.63$ μm. (c) The fitted line of reflectivity versus N_p when $\Lambda = 6.63$ μm.

To determine the above parameters, we simulate the reflection and transmission spectra of Bragg gratings with $N_p = 100$ and $N_p = 200$ at $\Lambda = 6.63$ μm by using the finite-difference time-domain (FDTD) method implemented in Lumerical software, as shown in Figs. 3(a) and 3(b). According to the simulation results, when $N_p = 100$, at the central wavelength of 1550 nm, the reflection and transmission are 63.3% and 7.9%, respectively. When $N_p = 200$, the reflection and transmission are 90.3% and 0.3%, respectively. As shown in Fig. 3(c), we simulate the relationship between N_p and reflectivity at the central wavelength under $\Lambda = 6.63$ μm. As can be seen from Fig. 3(c), the reflectivity increases from 35.7% to 99.5% as N_p increases from 50 to 350. The reflectivity is larger than 90.3% when $N_p \geq 200$.

3. Device fabrication and characterization

The WBG is fabricated using conventional UV lithography and wet etching processes based on the designed parameters. Optical microscope images of the fabricated WBG are shown in Fig. 4. The $\Lambda = 6.623$ μm, $W_1 = 8.026$ μm, and $W_2 = 3.214$ μm of the WBG are measured. The measured results are consistent with the designed values. Subsequently, to characterize the fabricated WBG, light emitted by a tunable laser source (TSL-550, Santec Corporation, Japan) is intro-

duced into the device through an edge-coupling system and single-mode optical fibers. The polarization state of the light is adjusted by a polarization controller. The output power is monitored by an optical power meter (MPM200, Santec Corporation, Japan).

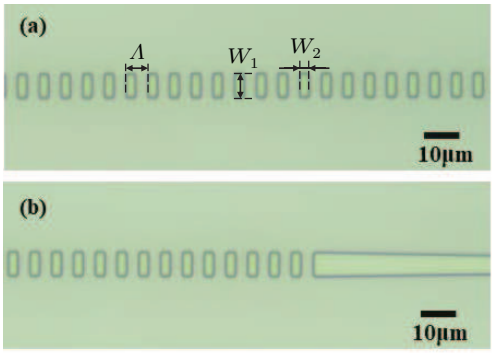


Fig. 4. (a) Optical microscope image of WBG. (b) Optical microscope image at transition section.

The transmission spectra of the fabricated WBG with $N_p = 100$ are shown in Fig. 5(a). We observe a resonance peak at 1544.22 nm. The *ER* and $\Delta\lambda_{3\,dB}$ of this resonance peak are measured to be 8.67 dB and 1.3 nm, respectively. The insertion loss is 18.4 dB (*IL*). This loss is jointly caused by the edge coupler, the fully etched grating structure, and the intrinsic absorption of the polymer. The loss of the straight waveguide on the same chip is approximately 15 dB (IL_1). The transmission loss per unit length of the straight waveguide is 3.14 dB/cm (IL_2).[17] Considering that the waveguide length is ~ 2.5 cm (L_1), we can calculate the propagation loss of the device waveguide according to

$$IL_3 = L_1 \cdot IL_2, \tag{10}$$

therefore, the propagation loss (IL_3) caused by absorption is 7.85 dB. We can calculate the coupling loss of the waveguide according to

$$IL_4 = IL_1 - IL_3. \tag{11}$$

The coupling loss (IL_4) is 7.15 dB. The transmission loss of the grating region is calculated by

$$IL_5 = IL_0 - IL_1. \tag{12}$$

The loss caused by the Bragg structure (IL_5) is 3.4 dB. This loss is attributed to the fully etched waveguide structure and the high-order grating design. In the active region of the device, we fabricate aluminum electrodes using a vacuum deposition process via thermal evaporation. The thickness of the electrodes can be controlled by adjusting the deposited aluminum amount and evaporation time. Subsequently, we achieve precise electrode patterning using UV lithography and wet etching techniques. When a voltage is applied to the electrodes, the temperature of the core layer changes due to Joule heating, which in turn alters the refractive index of the core layer, enabling thermo-optic modulation. We measure the current–voltage characteristic curve. As shown in Fig. 5(b), after linear fitting, the resistance of the heating electrode is calculated to be 101 Ω. The transmission spectra varying with voltage are shown in Fig. 5(a). It can be concluded that the central wavelength exhibits a blue shift with increasing voltage, which is consistent with the negative TOC of polymers. As shown in Fig. 5(c), it presents the linear fitting of the central wavelength of the WBG under different powers. The tuning efficiency of the WBG is −27.4 pm/mW.

Similarly, we also fabricate a Bragg grating with $N_p = 200$, while the remaining parameters are kept identical to those of the WBG with $N_p = 100$. As shown in Fig. 5(d), the transmission spectrum at $N_p = 200$ is presented, with λ being 1544.74 nm, $\Delta\lambda_{3\,dB}$ reaching 0.35 nm, *ER* approximately 26.3 dB, and insertion loss about 21.6 dB. Compared with the WBG at $N_p = 100$, although the central wavelength is almost unchanged, it exhibits a narrower bandwidth and a higher *ER*. Based on the test results, it is calculated that the WBG with $N_p = 200$ has a loss 3.2 dB higher than that with $N_p = 100$, which indicates that the trade-off between loss and *ER* should be carefully optimized. As shown in Fig. 5(e), we change the output voltage gradually from 0 to 5 V, continuously detect the current variation, obtain the current–voltage characteristic curve of this WBG, and calculate the resistance as 229 Ω. As shown in Figs. 5(d) and 5(f), transmission spectra of the WBG with $N_p = 200$ varying with voltage and the linear fitting of heating power and central wavelength are presented. The tuning efficiency of the WBG is −29.6 pm/mW. By comparing the measurement results of the grating with $N_p = 100$, we find that when the electrode length is doubled, the measured resistance doubles while the modulation efficiency remains nearly unchanged. It can be concluded that the electrode design affects the magnitude of the measured resistance but does not affect the modulation efficiency.

To investigate the relationship between the central wavelength and the period length, we fabricate and test WBGs with $N_p = 100$ and periods ranging from 6.59 μm to 6.69 μm with a step of 0.02 μm. The spectra are shown in Fig. 6(a). The $\Delta\lambda_{3\,dB}$ of the transmission peaks for each period length are identical. The *ER*s are all around 8 dB. The linear fitting between the period length and the central wavelength is shown in Fig. 6(b). The interval of adjacent period lengths is 0.02 μm, which results in a central wavelength shift of approximately 4.6 nm. We also fabricate WBGs with different numbers of periods (N_p) at a period length of 6.63 μm, as shown in Fig. 6(c), with central wavelengths all around 1544.7 nm. Meanwhile, in Fig. 6(d), we summarize the relationship between N_p and *ER* of the WBG order. When $N_p = 50$, *ER* is only 5.56 dB, while when $N_p = 200$, *ER* reaches up to 37.31 dB. It has been

verified that as N_p increases, *ER* increases and the reflectance at the central wavelength also increases, which is consistent with the result in Fig. 3(c).

Finally, we test the response time of the WBG when $N_p = 200$. A 250 Hz square wave signal is input through a signal generator (SDG6032X-E, Siglent), and a high-speed photodetector is connected to the output end. Meanwhile, the switching voltage is monitored using an oscilloscope. As shown in Fig. 7, the oscilloscope traces of the input drive signal and the output optical signal show that the response has a rise time (10%–90%) and a fall time (90%–10%), both of which are 280 μs.

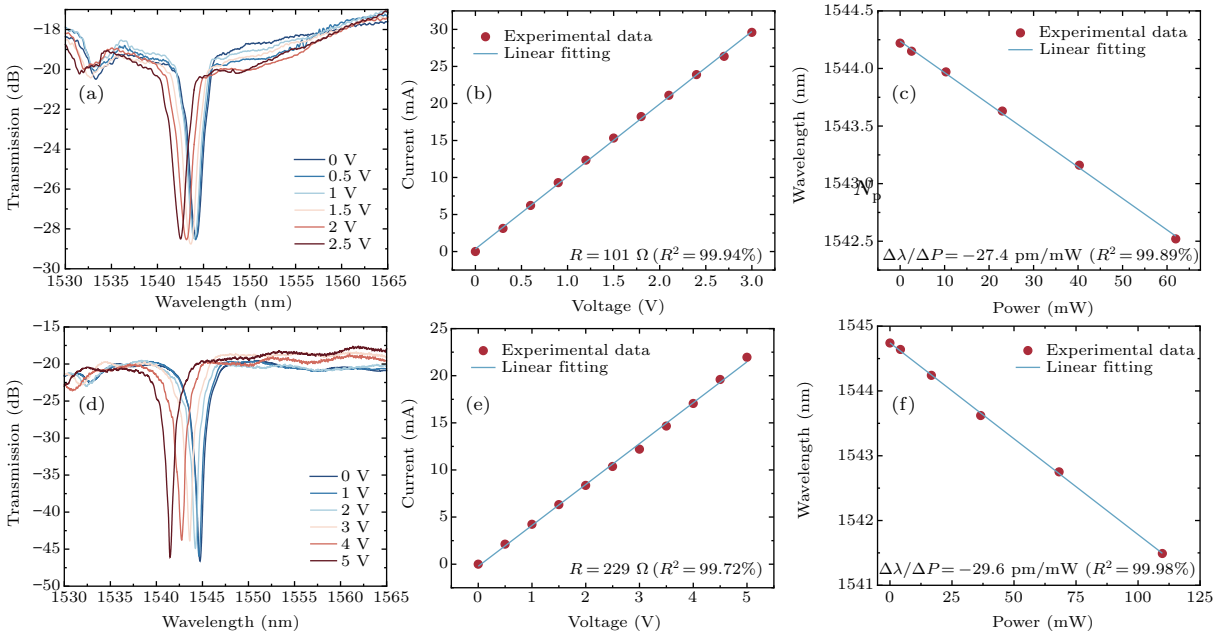


Fig. 5. (a) The normalized transmission spectrum with $N_p = 100$ after applying a voltage of 0–2.5 V; (b) the voltage–current (*U*–*I*) characteristic curve; (c) the thermal dependence fitting line of λ and the heating power *P*; (d) the normalized transmission spectrum with $N_p = 200$ after applying a voltage of 0–5 V; (e) the voltage–current (*U*–*I*) characteristic curve; (f) the thermal dependence fitting line of λ and the heating power *P*.

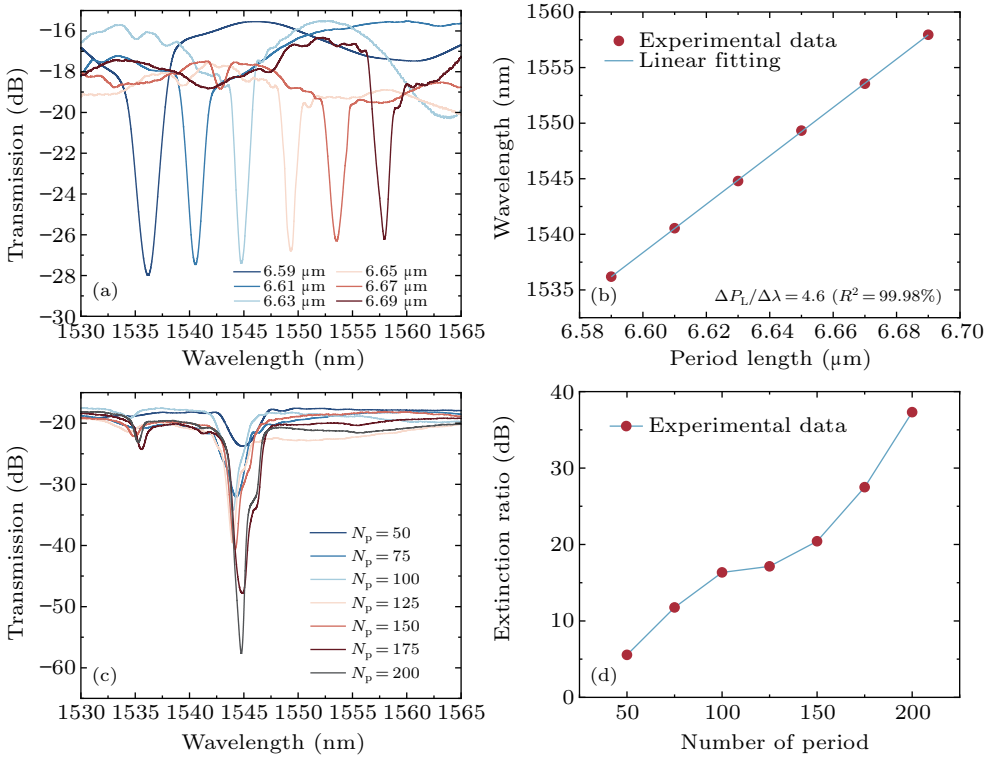


Fig. 6. (a) The transmission spectrum when $N_p = 100$ and Λ varies from 6.59 μm to 6.69 μm; (b) the fitting line of λ versus Λ; (c) at $\Lambda = 6.63$ μm, the transmission spectra with the number of periods $N_p = 50$–200; (d) the fitting curve of the extinction ratio versus N_p.

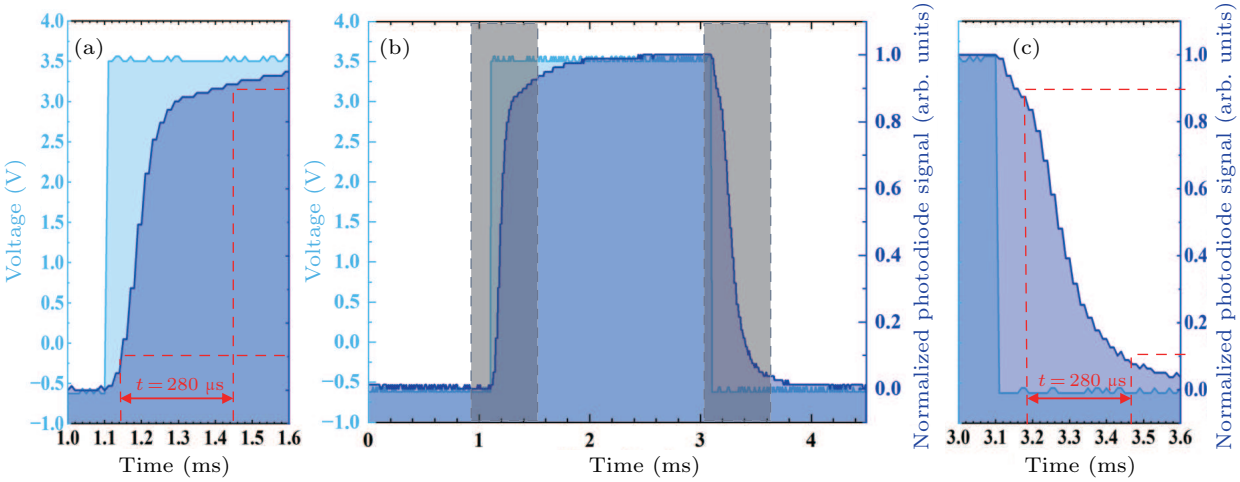


Fig. 7. The dynamic response curve of the WBG when a 250 Hz square-wave signal is applied to the electrode.

Table 2. Comparison of performance metrics for WBG filters and sensor.

Ref.	*ER* (dB)	$\lambda_{3\ \mathrm{dB}}$ (nm)	Tunable efficiency	Insertion loss (dB/mm)	Platform
[9]	12.8	0.9	−88 pm/°C*	–	polymer/silica
[21]	13	0.6	−160 pm/°C	1.2	polymer/silica
[22]	–	–	−425 pm/mW	–	polymer
[23]	22–27	6–26	160 pm/mW	1.0	SOI
Ours	26.3	0.35	−29.6 pm/mW	4.83	polymer/silica

*Calculated; –: Not mentioned

4. Discussion

Table 2 provides a comparison of performance metrics obtained in the present work with those reported for state-of-the-art WBG filters and sensors. In Ref. [9], a silica Bragg grating is demonstrated with polymer cladding. The polymer cladding improves the sensitivity to 88 pm/°C. To achieve a higher sensitivity, a polymer-core grating is fabricated in Ref. [21]. The sensitivity is twice that of a silica-core device. The add-drop structure is compact and useful for on-chip characterization. An impressive tuning efficiency of 425 pm/mW is achieved with buried electrodes and air trenches in Ref. [22]. However, the sidewall grating exhibits degraded spectra with significant noise due to waveguide sidewall roughness. On the SOI platform, fine structure engineering and compact footprint are attractive for grating design. By optimizing the corrugation depth, apodization strength, and grating length, the highest *ER* of 27 dB is achieved at 2 μm wavelength.[23] The WBG demonstrated in this work shows good performance in the spectrum. However, our grating still suffers from relatively high loss. To address this challenge, we propose that, compared with the traditional fully etched grating, a sidewall grating structure can better preserve the continuity of the waveguide core, allowing the optical field to remain confined within the core region. This design significantly reduces scattering loss in Bragg gratings. Therefore, optimizing the grating structure into a sidewall-type design may serve as a practical and feasible solution.[24] There is still ample room for improvement in tuning efficiency via electrode design and optimization. On the other hand, more complex grating designs, such as apodized gratings, are necessary for better spectral performance.

5. Summary

In conclusion, a high-order WBG filter is successfully optimized and experimentally demonstrated on a low-cost polymer/SiO_2 hybrid waveguide platform. The high order of the grating enables a larger period and reduces fabrication complexity. Using conventional UV lithography, the grating with 200 periods exhibits an *ER* of 26.3 dB with a 3-dB bandwidth of 0.35 nm at the central wavelength of 1544.74 nm. Owing to the high TOC of the polymer core, the tuning efficiency reaches −29.6 pm/mW. The dynamic response is 280 μs. The proposed WBG shows great potential for applications in optical switches, wavelength-division multiplexing, and sensing systems.

Acknowledgment

This work was supported by the National Key Research and Development Program of China (Grant No. 2024YFE0211800).

References

[1] Mori Y and Sato K 2021 *J. Opt. Commun. Netw.* **13** D43
[2] Sun C, Yin Y, Chen Z, Ye Y, Luo Y, Ma H, Wang L, Wei M, Jian J, Tang R, Dai H, Wu J, Li J, Zhang D, Lin H and Li L 2022 *PhotoniX* **3**, 12
[3] Zhang Z, Zhang S, Liu X, Wang Y, Chen H, Zhang D and Wang X 2024 *Laser Photonics Rev.* **18** 2400155
[4] Niu D, Wang L, Xu Q, Zhang Y, Chen H, Wang Y and Li X 2019 *Appl. Opt.* **58** 1276
[5] Tan Y and Dai D 2018 *J. Opt.* **20** 054004
[6] St-Yves J, Bahrami H, Jean P, LaRochelle S and Shi W 2015 *Opt. Lett.* **40** 5471
[7] Zhang W and Yao J 2018 *Nat. Commun.* **9** 1396

[8] Klitis C, Cantarella G, Strain M J and Sorel M 2015 *Proc. Conf. Ph. D. Res. Microelectron. Electron.* **2015** 7251408

[9] Park H, Lee H, Kim C, Ahn J H, Chung Y C and Oh D K 2006 *Jpn. J. Appl. Phys.* **45** L734

[10] Liu A, de Felipe D, Zawadzki C, Rizzo A, Biberman A, Bergman K and Osgood R M Jr 2018 *IEEE Photonics Technol. Lett.* **30** 1325

[11] Daniel P M, Manuel L G, Gonzalo W P J, Martín D P, Luque J M, Cheben P and Schmid J H 2021 *Opt. Express* **29** 15867

[12] Liang F, Zheng S, Zhao X, Wang H, Liu Y, Chen J and Dai D 2023 *J. Lightwave Technol.* **41** 7418

[13] Park T H, Kim S M and Oh M C 2020 *Opt. Express* **28** 10145

[14] Fathpour S 2015 *Nanophotonics* **4** 143

[15] Zhang Z, de Felipe D, Katopodis V, Kouloumentas C, Groumas P, Avramopoulos H, Dupuy J Y, Konczykowska A, Beretta A, Vannucci A, Cangini G, Dinu R, Schmidt D, Moehrle M, Runge P, Choi J H, Bach H G, Grote N, Keil N and Schell M 2015 *Photonics* **2** 1005

[16] Burke C S, Polerecky L and MacCraith B D 2004 *Meas. Sci. Technol.* **15** 1140

[17] Zeng G, Zhang D, Wang F, Wang X and Yin Y 2024 *Adv. Photonics Res.* **6** 2400118

[18] Yin Y, Yao M, Ding Y, Xu X, Li Y, Wu Y and Zhang D M 2022 *Micromachines.* **13** 511

[19] Shi W, Wang X, Lin C, Huang Y, Chen J, Zhang X and Yu J 2013 *Opt. Express* **21** 3633

[20] Liu Z, Zhong L, Liu S, Zhang Y, Wang J, Chen H and Zhang X 2024 *J. Semicond.* **45** 032401

[21] Tian L, Wang F, Wu Y D, Chen X, Wang Y, Zhang J and Dai D 2018 *Opt. Lett.* **43** 2348

[22] Liu A, Zhang Z, de Felipe D, Zawadzki C, Boes A, Lee B G and Osgood R M 2014 *IEEE Photonics Technol. Lett.* **26** 313

[23] Liu D, Wu H and Dai D 2019 *J. Lightwave Technol.* **37** 2217

[24] Prabhathan P, Murukeshan V M, Zhang J, Kumar R, Srinivasan B and Ong L S 2009 *Appl. Opt.* **48** 5598